2018-10-31

Mutations in influenza A virus neuraminidase and hemagglutinin confer resistance against a broadly neutralizing hemagglutinin stem antibody

Kristina L. Prachanronarong
University of Massachusetts Medical School

Et al.

Mutations in influenza A virus neuraminidase and hemagglutinin confer resistance against a broadly neutralizing hemagglutinin stem antibody

Kristina L. Prachanronarong[1#], Aneth S. Canale[1#], Ping Liu[2#], Mohan Somasundaran[1#], Shurong Hou[1], Yu-Ping Poh[4], Thomas Han[6], Quan Zhu[6], Nicholas Renzette[3], Konstantin B. Zeldovich[4], Timothy F. Kowalik[3], Nese Kurt-Yilmaz[1], Jeffrey D. Jensen[5], Daniel N. A. Bolon[1], Wayne A. Marasco[6], Robert W. Finberg[2], Celia A. Schiffer[1], Jennifer P. Wang[2]*

[1]Department of Biochemistry and Molecular Pharmacology, [2]Department of Medicine, [3]Department of Microbiology and Physiological Systems, [4]Program in Bioinformatics and Integrative Biology, University of Massachusetts Medical School, Worcester, Massachusetts, USA;

[5]School of Life Sciences, Center for Evolution & Medicine, Arizona State University, Tempe, Arizona, USA

[6]Department of Cancer Immunology and AIDS, Dana-Farber Cancer Institute, Department of Medicine, Harvard Medical School, Boston, Massachusetts, USA

Key words: hemagglutinin and neuraminidase mutants, resistance, broadly neutralizing antibody, influenza virus

[#]Kristina L. Prachanronarong, Aneth S. Canale, Ping Liu, and Mohan Somasundaran contributed equally to this work.

*Address correspondence to Jennifer P. Wang, jennifer.wang@umassmed.edu.

Present address: Jennifer P. Wang, Division of Infectious Diseases and Immunology, Department of Medicine, University of Massachusetts Medical School, Worcester, Massachusetts, USA

Abstract

Influenza A virus (IAV), a major cause of human morbidity and mortality, continuously evolves in response to selective pressures. Stem-directed, broadly neutralizing antibodies (sBnAbs) targeting influenza hemagglutinin (HA) are a promising therapeutic strategy, but neutralization escape mutants can develop. We used an integrated approach combining viral passaging, deep sequencing, and protein structural analyses to define escape mutations and mechanisms of neutralization escape *in vitro* for the F10 sBnAb. IAV was propagated with escalating concentrations of F10 over serial passages in cultured cells to select for escape mutations. Viral sequence analysis revealed three mutations in HA and one in neuraminidase (NA). Introduction of these specific mutations into IAV through reverse genetics confirmed their roles in resistance to F10. Structural analyses revealed that the selected HA mutations (S123G, N460S, and N203V) are away from the F10 epitope but may indirectly impact influenza receptor binding, endosomal fusion, or budding. The NA mutation E329K, which was previously identified to be associated with antibody escape, affects the active site of NA, highlighting the importance of the balance between HA and NA function for viral survival. Thus, whole genome population sequencing enables the identification of viral resistance mutations responding to antibody-induced selective pressure.

Importance

Influenza A virus is a public health threat for which currently available vaccines are not always effective. Broadly neutralizing antibodies that bind to the highly-conserved stem region of influenza hemagglutinin (HA) can neutralize many influenza strains. To understand how influenza virus can become resistant or "escape" such antibodies, we propagated influenza A virus *in vitro* with escalating concentrations of antibody and analyzed viral populations with whole genome sequencing. We identified HA mutations near and distal to the antibody binding epitope that conferred resistance to antibody neutralization. Additionally, we identified a neuraminidase (NA) mutation that allowed the virus to grow in the presence of high concentrations of the antibody. Virus carrying dual mutations in HA and NA also grew under high antibody concentrations. We show that NA mutations mediate the escape of neutralization by

49 antibodies against HA, highlighting the importance of a balance between HA and NA for optimal virus
50 function.

Introduction

Influenza A virus (IAV) causes a highly contagious acute respiratory illness in humans that is responsible for significant morbidity and mortality. IAV's unique combination of evolutionary mechanisms, including high mutation rate, segment reassortment, and shifts between multiple host species, pose significant challenges for controlling the disease and developing effective vaccinations. The influenza virion consists of eight negative-strand RNA segments which form protein-RNA complexes enveloped in a lipid membrane (1). These eight segments encode at least ten proteins known to be essential for infectivity and replication. The influenza polymerase lacks proofreading activity, resulting in a high spontaneous gene mutation rate (2). Within a given influenza strain, sequence evolution proceeds by mutation, selection, and genetic drift, all of which are affected by the host and by drug treatment. High mutation rates, together with development of influenza epidemics, make tracing the evolutionary history of the virus and discovering the principles governing IAV's evolution complex. Therefore a detailed understanding of IAV genome sequence evolution is imperative.

IAV has two surface glycoproteins, hemagglutinin (HA) and neuraminidase (NA). HA helps the viral genome enter the host cytoplasm through fusion of the viral membrane with the intracellular endosomal membrane (3). NA cleaves sialic acid from the host cell membrane during the release of newly formed viral progeny, thus reducing viral affinity for previously-infected cells (4). Eighteen different subtypes of influenza A HA (H1–H18) exist, which are divided into two distinct groups, group 1 (H1, H2, H5, H6, H8, H9, H11–H13, H16-H18) and group 2 (H3, H4, H7, H10, H14 and H15). HA is translated as a single polypeptide (HA0) that is cleaved by host proteases into HA1 and HA2 subunits, HA functions as a homo trimer composed of two copies of HA1 and one copy of HA2; the globular head (the receptor binding site) is formed by HA1, and the stem (or "stalk") region is formed by both HA2 and HA1 and is responsible for fusion [see (5) for review]. HA is the primary target of the humoral immune response during infection or vaccination. Influenza vaccines generally elicit strain-specific responses with antibodies that target the HA globular head, thereby limiting their efficacy and necessitating administration of new vaccines when a

novel strain becomes dominant.

Broadly neutralizing antibodies (BnAbs) bind to conserved epitopes on HA and can neutralize a wide spectrum of influenza viruses (6). In influenza, BnAb epitopes typically correspond to receptor binding and fusion machinery regions that are functionally conserved and thus less prone to mutation. BnAbs are potential therapeutic agents when used as passive immunotherapy and can also be integrated into the design of universal vaccines, which could provide protection against a broad range of influenza strains and be much more effective than current vaccines. BnAbs against the influenza receptor-binding site have limited neutralization capacity with each antibody effectively neutralizing a subset of strains in both groups 1 and 2 (6-8). Several stem-directed broadly neutralizing antibodies (sBnAbs) against highly conserved epitopes on the HA stem have been developed and characterized, including F10, C179, CR6261, which neutralize group 1 variants; CR8020, which neutralizes group 2 variants; and CR9114, 3I14, and 39.29, which neutralize both groups 1 and 2 (6, 9-11). sBnAbs that neutralize group 1 viruses share an epitope on the HA stem, while the epitope for group 2-specific antibodies is shifted toward the base of the HA stem. Structural analyses revealed that differences in the binding footprints are due to conformational constraints resulting from group-specific glycans on the HA stem (8).

sBnAbs prevent fusion of the host and virus membranes in the low pH of the endosome by locking HA in a pre-fusion conformation and preventing the extensive conformational changes in HA required for membrane fusion, blocking entry of viral RNA into the infected cell (8). Additional Fc-dependent mechanisms also contribute to protection *in vivo* (12). Despite the high conservation of sBnAbs epitopes in the HA stem region, neutralization escape mutations by sBnAbs have occurred in and around these epitopes (6, 13-17). Many of these mutations cause neutralization escape by directly reducing antibody binding affinity, but additional escape mechanisms that impact HA function or viral fitness may also emerge. A recent mutational scanning study of H1 HA has shown that single amino acid mutations are more likely to confer resistance against strain-specific antibodies that target the globular head of HA1 while similar mutations in the stalk confer only modest resistance to neutralization by sBnAbs (18). Another study

identified two escape mechanisms against a pan-IAV sBnAb, and some resistant viruses exhibited complete abolition of antibody binding while others showed enhanced fusion ability by HA (11). Defining such escape mechanisms is critical for evaluating sBnAbs to be incorporated into future vaccines and as therapeutic strategies.

The F10 antibody, a sBnAb derived from the *IGHV1-69* germline by panning immobilized HA using phage-display libraries generated from healthy donors, is broadly active against all group 1 viruses and protects mice from lethal H1N1 or H5N1 infection and reduces viral replication in lungs (9). sBnAbs such as F10 bind to highly-conserved regions of HA that are required for the virus to function, so characterizing sBnAb escape mutations that do not compromise virus survival provides insight for influenza biology. The goal of the current study was to identify IAV escape mutants for the sBnAb F10 by high throughput sequencing (HTS) analysis of virus populations generated through *in vitro* trajectory experiments. To select for escape mutants, we propagated the virus under the selective pressure of escalating concentrations of F10. Four mutations were identified, three in HA (none located in the F10 epitope) and one in NA, that were subsequently confirmed through reverse genetics to cause F10 resistance. A combination of structural and dynamic analyses reveal possible molecular mechanisms by which these mutations can confer F10 resistance. Thus, under the strict selective pressure of an antibody that targets an evolutionarily conserved and functionally critical region, influenza virus selects for indirect mechanisms of escape for survival.

Results

Serial passage of influenza A virus in the presence of F10

We tested F10 against influenza A/Brisbane/59/2007 (H1N1) virus in Madin-Darby canine kidney (MDCK) cells in our experimental trajectories (**Figure 1**). The A/Brisbane/59/2007 strain was used in the influenza vaccine in the United States for the 2008/2009 and 2009/2010 seasons (19). We passaged IAV under escalating concentrations of F10 monoclonal antibody, starting with 1X the 50% effective concentration (EC_{50}), or 0.3 μg/mL, at passage 4 and escalating to ≥5 μg/mL in MDCK cells to select for an

F10-resistant virus population in two independent trajectories, designated Experiments 1 & 2. Each experiment included a complete no-antibody control arm. In Experiment 2, we included an additional control with escalating concentrations of an irrelevant monoclonal antibody, 80R, specific to severe acute respiratory syndrome coronavirus (20) (**Figure 1A**). The amplification of virus over time is displayed in **Figure 1B**.

Sequence analysis reveals candidate F10 escape mutations

Analysis of HTS data from Experiments 1 & 2 using the Wright-Fisher ABC (WFABC) model identified viral mutations with a 99% posterior probability of being under positive selection (**Table 1**) (21, 22). These candidate F10 escape mutations included three non-synonymous mutations in segment 4 encoding HA: $N203V^{HA}$, $N460S^{HA}$, and $S123G^{HA}$ (H1 numbering system) and one non-synonymous mutation in segment 6 encoding NA, $E329K^{NA}$. The selection of $E329K^{NA}$ was observed in both trajectories with F10, but not with the 80R control. In addition, one non-synonymous mutation in segment 2, $A643T^{PB1}$, one non-synonymous mutation in segment 3, $L28P^{PA}$, and synonymous mutations in segments 4 and 5 were identified. The synonymous changes appear consistent with genetic hitchhiking effects associated with the above listed non-synonymous mutations, owing to their common trajectories. The allele frequencies increased with each passage, and none of these mutations were elicited with the irrelevant control 80R antibody or in the absence of antibody (**Figure 2A**). Selection coefficients are shown in **Figure 2B,** and the posterior estimates of effective population size (N_e) are shown in **Figure 2C**. As expected, N_e is reduced in the challenged population. Segment 4 mutations A638G and A639T generate a double mutant in perfect linkage to encode the $N203V^{HA}$ amino acid substitution.

F10 resistance validated by reverse genetics of individual mutant viruses

A reverse genetics approach was employed to generate influenza virus A/Brisbane/59/2007 bearing individual mutations $S123G^{HA}$, $N203V^{HA}$, $N460S^{HA}$, $E329K^{NA}$ and the oseltamivir resistance mutation $H275Y^{NA}$ (N1 numbering) as a control. Consistent with results from the serial passaging experiment, the

mutations S123G^{HA}, N203V^{HA}, N460S^{HA}, and E329K^{NA} each conferred resistance to F10 relative to wild type (WT), as demonstrated by higher viral titers in the presence of F10 (**Figure 3A**). The HA mutants (N460S^{HA}, S123G^{HA}, and N203V^{HA}) and NA mutant (E329K^{NA}) grew to higher titers than WT in the presence of >0.7 μg/mL of F10, while the control mutant H275Y^{NA} had titers comparable to that of WT virus. Of interest, the double mutant N203V^{HA}_E329K^{NA} had slightly higher titers at the intermediate concentration of 1.3 μg/mL of F10 than each mutant individually, suggesting that adaptation to F10 may involve a complex and concentration-dependent fitness landscape. EC_{50} and EC_{90} calculations revealed that all resistant mutations exhibited higher EC_{90} values compared to WT (**Table 2**), although the EC_{50} for the E329K^{NA} mutation was comparable to that of WT. The oseltamivir EC_{50} values for WT, E329K^{NA}, and H275Y^{NA} were also determined (**Figure 3B**). Oseltamivir EC_{50} values for WT, E329K^{NA}, and H275Y^{NA} are 0.2, 3.0, and 86.6 μM, respectively. E329K has been shown to reduce NA enzymatic activity relative to WT A/Brisbane/59/2007 (23), which is consistent with the increase of oseltamivir's effective concentration for E329K^{NA} compared to WT. Overall, the reverse genetics enabled generating virus harboring the individual selected mutations from *in vitro* passaging and confirming that these mutations confer resistance to F10.

We measured the plaque diameter of individually cloned viruses to determine the fitness of the identified escape mutations in HA and NA. In the absence of selection pressure by F10, the plaque sizes of N460S^{HA} and S123G^{HA} mutants were similar to that of WT. However, the plaque sizes of N203V^{HA} and E329K^{NA} were smaller than that of WT (**Figure 4**). This observation is consistent with studies that showed that the E329K^{NA} mutation, which was previously identified as important for antigenic drift, reduces NA enzyme activity and virus fitness (33). Plaques for the double mutant N203V^{HA}_E329K^{NA} were even smaller, possibly reflecting the effects of both mutations. Thus, while high titers of N203V^{HA} were observed in the presence of F10, N203V^{HA} appeared less fit based on plaque size.

Structural mapping of F10 escape mutants in HA

To further investigate the mutations selected in HA and identify escape mechanisms, we mapped the non-synonymous mutations $N460S^{HA}$, $S123G^{HA}$, and $N203V^{HA}$ onto available crystal structures. Notably, the mutations are located away from the F10 binding epitope (**Figure 5**). Instead of directly affecting F10 antibody binding, these distal mutations likely cause antibody escape through indirect mechanisms. Influenza RNA enters the host cell and the viral envelope and the endosomal membrane fuse. The N-terminal fragment of the HA2 subunit, or the fusion peptide, mediates fusion. At neutral pH, the fusion peptide is buried in a negatively-charged pocket in the stem of HA, but at acidic pH, the fusion peptide dissociates from the HA stem and inserts into the endosomal membrane to promote fusion between the viral membrane and the endosomal membrane (5, 24, 25).

Two non-synonymous HA mutations selected by the F10 antibody in Experiment 1, $N460S^{HA}$ and $S123G^{HA}$, are located at key positions involved in the conformational changes needed to facilitate membrane fusion (**Figure 5**). The side chain of N460 forms an intermonomer hydrogen bond adjacent to the fusion peptide which is broken when HA undergoes its conformational change upon fusion, thereby exposing N460 (**Figure 6**). N460 is the closest of the observed mutations to the F10 epitope on the HA stem, as residues 17-21 of the fusion peptide form the center of the F10 epitope. In the N460S, the shorter serine would be less likely to form this hydrogen bond and may alter the stability of the conformational change in HA (26, 27). S123 is located at a hinge region of the HA1 subunit (**Figure 7**). HA1 acts as a clamp on HA2 and stabilizes the metastable prefusion state of HA (28). Upon fusion, HA1 undergoes major conformational changes, one of which occurs around S123. In this region, an alpha helix begins to unfold altering the adjacent antiparallel beta-sheet that connects to the receptor binding subdomain (28). The mutation S123G introduces a flexible glycine residue into this hinge, which may facilitate this conformational change. Thus both $N460S^{HA}$ and $S123G^{HA}$ likely alter the conformational stability of HA.

The final observed mutation $N203V^{HA}$ is located at the receptor-binding site of HA (**Figure 8**). The emergence of $N203V^{HA}$ has been reported in influenza A/Brisbane/59/2007 during propagation of egg-derived virus in either MDCK or Vero cells (29). Residue 203 forms a hydrogen bond with the human

199 receptor analog LSTc in H2 HA (30), interacts with sialic acid through hydrogen bonds in H3 subtype
200 crystal structures (31, 32) and has been implicated in conferring receptor-binding specificity (33). The
201 selected mutation N203V^{HA} would result in the loss of any hydrogen bond with the receptor at this site.
202 Thus, N203V^{HA} could potentially alter receptor specificity and affinity.

203 ***Structural mapping of an F10 escape mutant in NA***

204 In addition to mutations in HA, a mutation in the IAV surface protein NA, E329K^{NA}, was selected
205 *in vitro* and confirmed to cause F10 resistance. Mutations at residue 329 have been previously reported in
206 response to selection with monoclonal antibodies (34-36). NA functions as a tetramer with substrate (sialic
207 acid) cleaving active site in each monomer. Residue 329 is located in a loop on the surface of NA, away
208 from both the tetramer interface and the active site. The E329K^{NA} substitution involves a charge switch
209 from an acidic to a basic side chain. To investigate the effects of the E329K^{NA} mutation on NA structure
210 and dynamics, the WT and E329K^{NA} NA tetramer structures of influenza A/Brisbane/59/2007 strain were
211 modeled and 100 ns molecular dynamics (MD) simulations performed as we have previously described to
212 interpret resistant mutations in NA (37) and other systems (38-41). The electrostatic surfaces of the two
213 variants were compared, as E329K^{NA} mutation constitutes an overall charge change of +8e^{-} for the
214 tetramer. Overall, the root mean square fluctuations (RMSFs, **Figure 9A, B**) of the active site in WT NA
215 were higher compared to E329K^{NA} variant, altering the dynamics of the active site. Interestingly, even
216 though the E329K^{NA} mutation is located far from the active site, the mutation had a distal effect and caused
217 the active site to become more positively charged (**Figure 9C, D**). Thus, the E329K^{NA} mutation had
218 propagating effects to alter the charge surface of the enzyme and fluctuations of the active sites, which may
219 underlie the decreased enzymatic activity previously reported for E329K^{NA} relative to WT
220 A/Brisbane/59/2007 (23). This alteration in substrate processing by NA may perturb the balance with HA
221 function and thus counter F10 inhibition.

222 **Discussion**

223 BnAbs against influenza have invigorated the influenza field given their potential use for universal
224 therapies and vaccines that protect against a broad spectrum of strains and subtypes. However, antibody
225 neutralization escape mutations can emerge, and understanding neutralization escape together with the
226 underlying molecular mechanisms is critical for designing antibodies that are less prone to resistance. Here,
227 we identified and characterized F10 escape mutations for a vaccine strain of influenza virus,
228 A/Brisbane/59/2007, by combining viral passaging, HTS, reverse genetics, and structural analyses. We had
229 previously applied a similar approach to understand the temporal evolution of oseltamivir resistance (21,
230 42), viral reassortment (43), and mutagenesis induced by favipiravir (44, 45). In our current results, we
231 identified mutations in regions of HA that confer virus neutralization (i.e., blockade of viral replication)
232 and may modulate receptor binding specificity or fusion (46) or viral budding and release of progeny. We
233 also confirm F10 resistance conferred by an NA mutation previously identified to drive antigenic drift (47).

234 The F10 escape mutations identified in HA are not located at the antibody epitope, and thus rather
235 than directly modulating antibody binding, these mutations instead cause antibody escape by indirect
236 mechanisms. Mutations at residues 460 and 123 are located in regions of HA that modulate the pH of
237 fusion (46). Residue N460 (residue 117 of HA2 in H3 numbering) is located in the stem region surrounding
238 the fusion peptide, and mutations at nearby residues 111, 112, and 114 (H3 numbering) had previously
239 been reported to increase the pH of fusion in H3, H5, and H7 subtypes (30, 46, 48, 49). Many other
240 mutations in the fusion peptide or the surrounding pocket have also been shown to significantly affect the
241 fusion activity of HA or the pH of membrane fusion (30, 46, 48-51). Residue S123 (residue 113 in H3
242 numbering) is located in a 110-helix that is involved in the reorganization of the HA1-HA2 interface that
243 occurs during membrane fusion, and mutations at residues 104, 110, and 115 (in H3 numbering) can impact
244 the pH of fusion due to changes at the HA1-HA2 interface (46, 52). Mutations at residue 203 (190 in H3
245 numbering) have been reported to impact receptor specificity for substrates with an α-2,3 or α-2,6
246 glycosidic linkage between the terminal sialic acid and the adjacent carbohydrate (47, 53-56). For instance,
247 the mutation $E190D^{HA}$ in combination with $G225D^{HA}$ (H3 numbering) in H1 increases specificity for α-2,6

248 linked sialic acids and reduces affinity for α-2,3 linked sialic acids (56). Such mutations that alter receptor-
249 binding affinity are selected in response to other neutralizing antibodies as well (57, 58). Overall, we found
250 that under the selective pressure of a sBnAb that has a highly conserved epitope, mutations distal to the
251 antibody binding epitope in HA are selected to enable antibody escape.

252 In addition to mutations in HA, we found a mutation in NA that confers F10 resistance. This
253 E329K^{NA} mutation in influenza A/Brisbane/59/2007 was previously described in the antigenic evolution of
254 proteins in H1N1 viruses used in vaccine formulations during the last 15 years through analysis of
255 inhibition titers and antigenic cartography (47). This single point mutation was found to be primarily
256 responsible for the lack of inhibition by polyclonal antibodies specific for an earlier influenza vaccine
257 antigen, impacting NA drift. Although antigenic change and drift in NA are often due to antibody selection,
258 antigenic change in NA may also result from a functional change in HA so as to maintain the functional
259 balance between HA and NA that is essential for optimal virus infectivity (59). Our structural analyses here
260 revealed the molecular mechanism by which the distal E329K mutation impacts the NA active site, likely
261 modulating enzymatic activity and the functional HA/NA balance in conferring F10 neutralization escape
262 of IAV. Our data demonstrate the plasticity of escape and the emergence of strong, off-target resistance via
263 the NA protein.

264 A closer inspection of experimental trajectories suggests that the E329K^{NA} mutation may confer
265 resistance against F10 in combination with N203V^{HA}. Once the E329K^{NA} mutation with reduced NA
266 activity emerges and reaches a high frequency in the population (**Figure 2A, P5 in Experiment 1**), the
267 appearance of the N203V^{HA} mutation restores the HA-NA functional balance and the drug pressure is
268 effectively reduced thus allowing for further fine-tuning of resistance. These mutations occur in the
269 opposite order in Experiment 2, in which N203V^{HA} reaches a high frequency at P7, then E329K^{NA} reaches
270 a similarly high frequency at P10-11 (see **Figure 2A**). That both trajectories finally stabilized with the two
271 mutations N203V^{HA} and E329K^{NA} suggests that there is an interdependence in conferring resistance to F10.
272 A similar pattern of drug resistance was described by Ginting et al. (60), wherein H275Y^{NA} functioned in

concert with mutations in HA to mediate oseltamivir resistance. These observations highlight potential intergenic epistatic interactions between HA and NA, which interact with the same molecule, sialic acid, on host receptors but have antagonistic functions. Interestingly, the average plaque size of virus containing both $N203V^{HA}$_$E329K^{NA}$ was smaller than viruses containing the individual mutants. The molecular mechanism of neutralization escape demonstrates the plasticity of escape and the emergence of strong, off-target resistance via the NA protein. The ability of mutant NA to bind HA receptors is demonstrated *in vitro*, which suggests that HA receptor-binding function can be supplanted by an appropriately evolved NA (61).

These results also highlight the role of both genetic drift and genetic hitchhiking in determining patterns of sequence evolution in IAV. Notably, a number of mutations identified as positively selected in the presence of F10 were also found to be segregating in the control populations (*e.g.*, A638G and the linked mutation A639T, as well as T1148C). By chance, these mutations were seeded at an intermediate frequency in the starting populations, and their subsequent dynamics in the control are consistent with genetic drift (*i.e.*, fluctuating across passages). Conversely, the frequency dynamics observed in the presence of F10 are consistent with positive selection. Relatedly, a small number of synonymous mutations were also observed to similarly increase in frequency. However, their overlapping allele frequency trajectories with the identified non-synonymous mutations strongly suggest linked, rather than direct, selection (i.e., genetic hitchhiking).

In summary, we identified mutations at HA and NA that promote resistance to the sBnAb F10 *in vitro*. Our results provide further evidence that mutations in one of these functionally complementary proteins in IAV can facilitate mutations in the other thus shaping the evolutionary landscape of the virus (62). While the serial passaging and HTS approaches may fail to distinguish functionally interacting mutations from those simply linked by genetic hitchhiking effects (that is, a beneficial mutation linked to an otherwise neutral, or even weakly deleterious, mutation), mutant viruses individually generated by reverse genetics confirmed a functional interplay between $N203V^{HA}$ and $E329K^{NA}$. This result highlights

298 the importance of considering not only focal point mutations, but also the variable fitness effects induced
299 by the genetic backgrounds on which those mutations occur. IAV can use diverse and indirect molecular
300 mechanisms to escape neutralization by sBnAbs. An in-depth understanding of genome-wide effects of
301 sBnAbs on different IAV subtypes will yield insights on which "universal" influenza vaccines may be the
302 most effective and least likely to induce escape mutants. Furthermore, additive and synergistic effects of
303 single and combinations of HA and NA mutations on virus replication in the presence and absence of
304 antiviral drugs and sBnAbs can be monitored to define and quantify the impact of multiple selective
305 pressures on the evolution of resistance over time. Given that these will be "real world" pressures faced by
306 IAV, such combination studies will be invaluable for determining which combinations may serve as
307 optimal therapeutic strategies in treating future epidemics and pandemics.

308 **Materials and Methods**

309 ***Cells, virus stocks, and chemicals.*** Madin-Darby canine kidney (MDCK) cells were obtained from
310 American Type Culture Collection (Manassas, VA) and propagated in Eagle's minimal essential medium
311 (MEM) with 10% fetal bovine serum (FBS; Hyclone, Logan, UT) and 2 mM penicillin/streptomycin.
312 Influenza virus A/Brisbane/59/2007 (H1N1), grown in chicken egg allantoic fluid, was obtained through
313 the NIH Biodefense and Emerging Infections Research Resources Repository, NIAID, NIH (NR-12282; lot
314 58550257) and passaged three times in MDCK cells (passages 1–3). Oseltamivir carboxylate was obtained
315 from Roche (F. Hoffmann-La Roche Ltd, Basel, Switzerland).

316 ***Viral titer determination by plaque assay.*** Viruses were quantified on MDCK cells to determine infectious
317 titer (plaque forming units per mL, or PFU/mL) as previously described (63). In brief, six 10-fold serial
318 dilutions were performed on the viral samples followed by 1 h of binding at 37 °C on confluent MDCK
319 cells in 12-well plates. After washing off unbound virus with phosphate buffered saline (PBS), the cells
320 were overlaid with agar (0.5%) in DMEM-F12 supplemented with penicillin/streptomycin, L-glutamine,
321 bovine serum albumin, HEPES, sodium bicarbonate, and 20 µg/mL acetylated trypsin (Sigma, St. Louis,

MO). After the agar solidified, the plates were incubated for ~48 h at 37 °C. Cells were fixed and stained with primary antibody anti-H1 (MAB8261, Millipore, Billerica, MA). Plaques were visualized with anti-mouse horseradish peroxidase-conjugated secondary antibody (BD Biosciences, San Jose, CA) and developed with peroxidase substrate kit (Vector Laboratories, Burlingame, CA).

Viral culture. Viruses were serially passaged in MDCK cells (2.5 x 10^5 cells/well). The MOI for passages was 0.01 except for late passages in the first experiment, for which output virus was low and MOI was adjusted to accommodate. Trajectories were prepared both in the presence and absence of escalating concentrations of F10 antibody or equivalent concentrations of the control monoclonal antibody 80R. In passage 4, the antibody concentration was 1X the EC_{50}. For the next passage, the concentration was increased to 2X the EC_{50}, and then doubled for each subsequent passage as long as >50% cytopathic effect (CPE) was present. If <50% CPE was present, the concentration of antibody was escalated at a slower rate.

Determination of the EC_{50} and EC_{90} for F10 antibody. The EC_{50} and EC_{90} values were defined as the concentration of antibody that reduced plaque number to 50% or 90% of no drug control, respectively. In brief, 3 x 10^4 MDCK cells/well were seeded in a 96-well plate and incubated overnight at 37 °C, 5% CO_2. Virus was added to cells at a multiplicity of infection (MOI) of 0.01 in 50 µL of influenza virus growth medium [EMEM/10% FBS with 2 mM penicillin/streptomycin, 7.5% bovine serum albumin, and 1 µg/mL TPCK-treated-trypsin (Sigma)] plus serial dilutions of F10 antibody. After incubation at 37 °C for 1 h, cells were washed once with PBS; 200 µL of influenza virus growth medium with the appropriate concentration of antibody was added and cells were again incubated at 37 °C for several days. Supernatants were collected when >90% CPE was achieved for at least one antibody concentration. Supernatants were centrifuged for 15 min at 300 × *g* at 4 °C and stored at -80 °C. The viral titer for each sample was determined by plaque assay. Resulting data were fit to a standard binding equation (variable slope, four parameters) in order to estimate EC_{50} and EC_{90} values with GraphPad Prism Version 7 (La Jolla, CA).

High-throughput sequencing. We developed a high-throughput sample processing workflow, carried out in a 96-well format, including RNA purification, reverse transcription, whole genome PCR, followed by DNA barcoding and library preparation, as previously described (42). Libraries were sequenced on the Illumina HiSeq2000 platform to generate 100 nucleotide reads.

Bioinformatics analysis. An integrated bioinformatics pipeline was developed to trim and bin the raw read data based on barcode, align reads to the reference IAV genome, and quantify the level of nucleotide and amino acid variability within the viral population, as previously described (21, 42). To streamline the processing of large numbers of IAV samples, an SQL database with a web interface was developed, integrating sample growth conditions with DNA barcoding information. The database was directly accessed using the analysis pipeline, eliminating the potential of human error when correlating experimental conditions with large scale IAV genomic data.

Short reads from the Illumina platform were filtered for quality scores >20 throughout the read and aligned to the strain's reference genome using BLAST. Over 95% of the selected reads could be mapped to the IAV reference genome obtained from GenBank (accessions CY030232, CY031391, CY058484-CY058486, CY058488-CY058489, CY058491). Only alignments longer than 80 nucleotides were retained. The median sequencing depth was 14,400. Amino acid frequencies were calculated after aligning translated reads to the corresponding positions in the reference proteins. Unfolded single nucleotide polymorphism (SNP) frequencies were generated using the IAV reference genome and used for the population genetics analyses and the amino acid frequencies were used for the structural analysis. The sequencing datasets generated in this study are available at http://bib.umassmed.edu/influenza.

Population genetic analysis. To distinguish SNPs putatively evolving under positive selection from those evolving under genetic drift alone, we applied the Wright-Fisher ABC approach (see the software page of: http://jjensenlab.org) to estimate a global effective population size (N_e) and per site selection coefficients (s) based on the allele frequency trajectories through time (21, 22, 42). We considered all trajectories

reaching a frequency of at least 2% in any passage. If at least 99% of the posterior probability density of the selection coefficient for a given SNP was positive, the site was considered to be significant.

Structural analyses and simulations. The amino acid sequence of influenza A/Brisbane/59/2007 (H1N1) HA was obtained from UniProt using the accession number B0VX46, which is associated with the GenBank accession number CY030232. This HA sequence was aligned to the amino acid sequences of published crystal structures to determine the location of specific mutations on the structure of HA, and the possible impact of these mutations was determined based on what has been reported in the literature about HA structure, conformational changes in HA that occur during fusion, and HA receptor binding. The published crystal structures used in this analysis include F10 in complex with H5 HA (PDB ID: 3FKU), H1 HA bound to the human receptor analog sialylneolacto-N-tetraose c (LSTc) (PDB ID: 2WRG), a solubilized trimeric H3 HA at the pH of membrane fusion (PDB ID: 1HTM), and H2 HA at neutral and acidic pH (PDB ID: 3QQB, 3QQO). The mutagenesis wizard in PyMOL was used to mutate residue 203 to an asparagine in two crystal structures to match the A/Brisbane/59/2007 (H1N1) HA sequence (PDB ID: 3FKU, 2WRG) (64). NA from influenza A/Brisbane/59/2007 strain WT and E329K^{NA} apo structures were modeled based on N1-oseltamivir co-crystal structure (PDB: 3CL2) through the program Modeller 9.15.

All molecular dynamics simulations were performed using Desmond (65) from Schrodinger. The models were first optimized using Protein Preparation Wizard. The simulation systems were then built through Desmond System Setup using OPLS3 force field (66). SPC solvation model was used with cubic boundary conditions and 12 Å buffer box size. The final system was neutral and had 0.15 M NaCl. A multi-stage MD simulation protocol was used, as previously described (67). All simulations were performed for a total of 100 ns. The RMSF of protein backbone and DNA molecule as well as the protein-ligand contact diagrams were calculated using in-house modified Schrodinger trajectory analysis python scripts. The electrostatic surface calculations of the final frame in MD simulations were done through PyMol APBS plugin.

Reverse genetics and viral rescue. The full-length complementary DNA (eight segments) of Brisbane/59/2007 virus that were cloned into the pHW2000 plasmid vector to generate reverse-genetics viruses were obtained from R. Webby (St. Jude Children's Research Hospital, Memphis, TN). Mutations of interest were introduced into the corresponding HA and NA genes by using QuikChange site-directed mutagenesis (Agilent). Sanger sequencing was used to confirm the presence of these mutants. Reverse-genetics viruses were rescued by transfecting a co-culture of 293T/MDCK cells with eight pHW2000 plasmids containing the eight virus segments, using TransIT LT-1 (Mirus Bio), as described previously (8 segments, 7 + 1: wt + mutant, or 6+2:wt + double mutant). Rescued P2 virus was sequenced and confirmed as containing the correct variant NA segment in the uniform backbone from other seven segments of Brisbane/59/2007. Stocks of viruses harvested from infected MDCK cells were titrated by plaque assay. These stocks were used to evaluate viral fitness/growth, and for determining EC_{50} and EC_{90} values for oseltamivir and F10. Images of plaques were acquired using a Nikon SMZ1500 microscope. For each mutant, we used the NIS Elements-BR Analysis program to measure the diameter of 20 randomly selected plaques. The average plaque size for each mutant was calculated and used as an estimate of growth rate.

Acknowledgments

We thank Melanie Trombly for assistance with manuscript preparation and R. Webby for A/Brisbane/59/2007 virus constructs for reverse genetics. This work was supported by the Office of the Assistant Secretary of Defense for Health Affairs, through the Peer Reviewed Medical Research Program (Award No. W81XWH-15-1-0317) and by the Defense Advanced Research Projects Agency (DARPA) Prophecy Program, Defense Sciences Office (DSO), Contract No. HR0011-11-C-0095 and D13AP00041. Opinions, interpretations, conclusions and recommendations are those of the author and are not necessarily endorsed by the Department of Defense.

A.S.C., K.B.Z., N.R., T.F.K., D.N.A.B., J.D.J., W.A.M., R.W.F., C.A.S., and J.P.W. designed the research; K.L.P., P.L., M.S., K.B.Z., Y.-P.P., S.H., and N.R. performed the research; T.H., Q.Z., and

Journal of Virology

JVI

Journal of Virology

417 W.A.M. contributed new reagents/analytic tools and contributed to data interpretation; K.L.P., A.S.C., P.L,

418 N.K.-Y. and J.P.W. contributed to the analysis and wrote the paper.

419 There are no conflicts of interest.

420 **References**

421

422 1. **Palese P, Shaw M.** 2007. Orthomyxoviridae: the viruses and their replication. *In* Knipe D, Howley
423 P (ed), Fields Virology. Lippincott Williams & Wilkins, Philadelphia.

424 2. **Drake JW.** 1993. Rates of spontaneous mutation among RNA viruses. Proc Natl Acad Sci U S A
425 **90:**4171-4175.

426 3. **White J, Hoffman L, Arevalo J, Wilson I.** 1997. Attachment and entry of influenza virus into host
427 cells. Pivotal roles of hemagglutinin, p pp. 80–104. *In* W C, RM B, RL G (ed), Structural Biology
428 of Viruses. Oxford University Press.

429 4. **Wagner R, Matrosovich M, Klenk HD.** 2002. Functional balance between haemagglutinin and
430 neuraminidase in influenza virus infections. Rev Med Virol **12:**159-166.

431 5. **Wilson IA, Skehel JJ, Wiley DC.** 1981. Structure of the haemagglutinin membrane glycoprotein of
432 influenza virus at 3 A resolution. Nature **289:**366-373.

433 6. **Laursen NS, Wilson IA.** 2013. Broadly neutralizing antibodies against influenza viruses. Antiviral
434 Res **98:**476-483.

435 7. **Burton DR, Poignard P, Stanfield RL, Wilson IA.** 2012. Broadly neutralizing antibodies present
436 new prospects to counter highly antigenically diverse viruses. Science **337:**183-186.

437 8. **Corti D, Cameroni E, Guarino B, Kallewaard NL, Zhu Q, Lanzavecchia A.** 2017. Tackling
438 influenza with broadly neutralizing antibodies. Curr Opin Virol **24:**60-69.

439 9. **Sui J, Hwang WC, Perez S, Wei G, Aird D, Chen LM, Santelli E, Stec B, Cadwell G, Ali M,**
440 **Wan H, Murakami A, Yammanuru A, Han T, Cox NJ, Bankston LA, Donis RO, Liddington**
441 **RC, Marasco WA.** 2009. Structural and functional bases for broad-spectrum neutralization of avian
442 and human influenza A viruses. Nat Struct Mol Biol **16:**265-273.

10. **Fu Y, Zhang Z, Sheehan J, Avnir Y, Ridenour C, Sachnik T, Sun J, Hossain MJ, Chen LM, Zhu Q, Donis RO, Marasco WA.** 2016. A broadly neutralizing anti-influenza antibody reveals ongoing capacity of haemagglutinin-specific memory B cells to evolve. Nat Commun **7:**12780.

11. **Chai N, Swem LR, Reichelt M, Chen-Harris H, Luis E, Park S, Fouts A, Lupardus P, Wu TD, Li O, McBride J, Lawrence M, Xu M, Tan MW.** 2016. Two Escape Mechanisms of Influenza A Virus to a Broadly Neutralizing Stalk-Binding Antibody. PLoS Pathog **12:**e1005702.

12. **Bournazos S, DiLillo DJ, Ravetch JV.** 2015. The role of Fc-FcgammaR interactions in IgG-mediated microbial neutralization. J Exp Med **212:**1361-1369.

13. **Friesen RH, Lee PS, Stoop EJ, Hoffman RM, Ekiert DC, Bhabha G, Yu W, Juraszek J, Koudstaal W, Jongeneelen M, Korse HJ, Ophorst C, Brinkman-van der Linden EC, Throsby M, Kwakkenbos MJ, Bakker AQ, Beaumont T, Spits H, Kwaks T, Vogels R, Ward AB, Goudsmit J, Wilson IA.** 2014. A common solution to group 2 influenza virus neutralization. Proc Natl Acad Sci U S A **111:**445-450.

14. **Throsby M, van den Brink E, Jongeneelen M, Poon LL, Alard P, Cornelissen L, Bakker A, Cox F, van Deventer E, Guan Y, Cinatl J, ter Meulen J, Lasters I, Carsetti R, Peiris M, de Kruif J, Goudsmit J.** 2008. Heterosubtypic neutralizing monoclonal antibodies cross-protective against H5N1 and H1N1 recovered from human IgM+ memory B cells. PLoS One **3:**e3942.

15. **Han T, Marasco WA.** 2011. Structural basis of influenza virus neutralization. Ann N Y Acad Sci **1217:**178-190.

16. **Dreyfus C, Ekiert DC, Wilson IA.** 2013. Structure of a classical broadly neutralizing stem antibody in complex with a pandemic H2 influenza virus hemagglutinin. J Virol **87:**7149-7154.

17. **Ekiert DC, Friesen RH, Bhabha G, Kwaks T, Jongeneelen M, Yu W, Ophorst C, Cox F, Korse HJ, Brandenburg B, Vogels R, Brakenhoff JP, Kompier R, Koldijk MH, Cornelissen LA, Poon LL, Peiris M, Koudstaal W, Wilson IA, Goudsmit J.** 2011. A highly conserved neutralizing epitope on group 2 influenza A viruses. Science **333:**843-850.

18. **Doud MB, Lee JM, Bloom JD.** 2018. How single mutations affect viral escape from broad and narrow antibodies to H1 influenza hemagglutinin. Nat Commun **9:**1386.

19. **Barr IG, McCauley J, Cox N, Daniels R, Engelhardt OG, Fukuda K, Grohmann G, Hay A, Kelso A, Klimov A, Odagiri T, Smith D, Russell C, Tashiro M, Webby R, Wood J, Ye Z, Zhang W.** 2010. Epidemiological, antigenic and genetic characteristics of seasonal influenza A(H1N1), A(H3N2) and B influenza viruses: basis for the WHO recommendation on the composition of influenza vaccines for use in the 2009-2010 northern hemisphere season. Vaccine **28:**1156-1167.

20. **Sui J, Li W, Murakami A, Tamin A, Matthews LJ, Wong SK, Moore MJ, Tallarico AS, Olurinde M, Choe H, Anderson LJ, Bellini WJ, Farzan M, Marasco WA.** 2004. Potent neutralization of severe acute respiratory syndrome (SARS) coronavirus by a human mAb to S1 protein that blocks receptor association. Proc Natl Acad Sci U S A **101:**2536-2541.

21. **Foll M, Poh YP, Renzette N, Ferrer-Admetlla A, Bank C, Shim H, Malaspinas AS, Ewing G, Liu P, Wegmann D, Caffrey DR, Zeldovich KB, Bolon DN, Wang JP, Kowalik TF, Schiffer CA, Finberg RW, Jensen JD.** 2014. Influenza virus drug resistance: a time-sampled population genetics perspective. PLoS Genet **10:**e1004185.

22. **Foll M, Shim H, Jensen JD.** 2015. WFABC: a Wright-Fisher ABC-based approach for inferring effective population sizes and selection coefficients from time-sampled data. Mol Ecol Resour **15:**87-98.

23. **Duan S, Govorkova EA, Bahl J, Zaraket H, Baranovich T, Seiler P, Prevost K, Webster RG, Webby RJ.** 2014. Epistatic interactions between neuraminidase mutations facilitated the emergence of the oseltamivir-resistant H1N1 influenza viruses. Nat Commun **5:**5029.

24. **Bullough PA, Hughson FM, Skehel JJ, Wiley DC.** 1994. Structure of influenza haemagglutinin at the pH of membrane fusion. Nature **371:**37-43.

25. **Wilschat JC, McElhaney JE, Palache AM.** 2006. Influenza Rapid Reference, 2 ed. Mosby-Elsevier Science, London.

26. **Daniels RS, Downie JC, Hay AJ, Knossow M, Skehel JJ, Wang ML, Wiley DC.** 1985. Fusion mutants of the influenza virus hemagglutinin glycoprotein. Cell **40:**431-439.

27. **Ivanovic T, Choi JL, Whelan SP, van Oijen AM, Harrison SC.** 2013. Influenza-virus membrane fusion by cooperative fold-back of stochastically induced hemagglutinin intermediates. Elife **2:**e00333.

28. **Xu R, Wilson IA.** 2011. Structural characterization of an early fusion intermediate of influenza virus hemagglutinin. J Virol **85:**5172-5182.

29. **Nakowitsch S, Waltenberger AM, Wressnigg N, Ferstl N, Triendl A, Kiefmann B, Montomoli E, Lapini G, Sergeeva M, Muster T, Romanova JR.** 2014. Egg- or cell culture-derived hemagglutinin mutations impair virus stability and antigen content of inactivated influenza vaccines. Biotechnol J **9:**405-414.

30. **Liu J, Stevens DJ, Haire LF, Walker PA, Coombs PJ, Russell RJ, Gamblin SJ, Skehel JJ.** 2009. Structures of receptor complexes formed by hemagglutinins from the Asian Influenza pandemic of 1957. Proc Natl Acad Sci U S A **106:**17175-17180.

31. **Eisen MB, Sabesan S, Skehel JJ, Wiley DC.** 1997. Binding of the influenza A virus to cell-surface receptors: structures of five hemagglutinin-sialyloligosaccharide complexes determined by X-ray crystallography. Virology **232:**19-31.

32. **Weis W, Brown JH, Cusack S, Paulson JC, Skehel JJ, Wiley DC.** 1988. Structure of the influenza virus haemagglutinin complexed with its receptor, sialic acid. Nature **333:**426-431.

33. **Tumpey TM, Maines TR, Van Hoeven N, Glaser L, Solorzano A, Pappas C, Cox NJ, Swayne DE, Palese P, Katz JM, Garcia-Sastre A.** 2007. A two-amino acid change in the hemagglutinin of the 1918 influenza virus abolishes transmission. Science **315:**655-659.

34. **Air GM, Els MC, Brown LE, Laver WG, Webster RG.** 1985. Location of antigenic sites on the three-dimensional structure of the influenza N2 virus neuraminidase. Virology **145:**237-248.

35. **Air GM, Laver WG, Webster RG, Els MC, Luo M.** 1989. Antibody recognition of the influenza virus neuraminidase. Cold Spring Harb Symp Quant Biol **54 Pt 1:**247-255.

36. **Webster RG, Air GM, Metzger DW, Colman PM, Varghese JN, Baker AT, Laver WG.** 1987. Antigenic structure and variation in an influenza virus N9 neuraminidase. J Virol **61:**2910-2916.

37. **Prachanronarong KL, Ozen A, Thayer KM, Yilmaz LS, Zeldovich KB, Bolon DN, Kowalik TF, Jensen JD, Finberg RW, Wang JP, Kurt-Yilmaz N, Schiffer CA.** 2016. Molecular Basis for Differential Patterns of Drug Resistance in Influenza N1 and N2 Neuraminidase. J Chem Theory Comput **12:**6098-6108.

38. **Soumana DI, Kurt Yilmaz N, Ali A, Prachanronarong KL, Schiffer CA.** 2016. Molecular and Dynamic Mechanism Underlying Drug Resistance in Genotype 3 Hepatitis C NS3/4A Protease. J Am Chem Soc **138:**11850-11859.

39. **Lin KH, Ali A, Rusere L, Soumana DI, Kurt Yilmaz N, Schiffer CA.** 2017. Dengue Virus NS2B/NS3 Protease Inhibitors Exploiting the Prime Side. J Virol **91**.

40. **Ozen A, Lin KH, Kurt Yilmaz N, Schiffer CA.** 2014. Structural basis and distal effects of Gag substrate coevolution in drug resistance to HIV-1 protease. Proc Natl Acad Sci U S A **111:**15993-15998.

41. **Ragland DA, Nalivaika EA, Nalam MN, Prachanronarong KL, Cao H, Bandaranayake RM, Cai Y, Kurt-Yilmaz N, Schiffer CA.** 2014. Drug resistance conferred by mutations outside the active site through alterations in the dynamic and structural ensemble of HIV-1 protease. J Am Chem Soc **136:**11956-11963.

42. **Renzette N, Caffrey DR, Zeldovich KB, Liu P, Gallagher GR, Aiello D, Porter AJ, Kurt-Jones EA, Bolon DN, Poh YP, Jensen JD, Schiffer CA, Kowalik TF, Finberg RW, Wang JP.** 2014.

Evolution of the influenza A virus genome during development of oseltamivir resistance in vitro. J Virol **88:**272-281.

43. **Zeldovich KB, Liu P, Renzette N, Foll M, Pham ST, Venev SV, Gallagher GR, Bolon DN, Kurt-Jones EA, Jensen JD, Caffrey DR, Schiffer CA, Kowalik TF, Wang JP, Finberg RW.** 2015. Positive Selection Drives Preferred Segment Combinations During Influenza Virus Reassortment. Mol Biol Evol **32:**1519-1532.

44. **Bank C, Renzette N, Liu P, Matuszewski S, Shim H, Foll M, Bolon DN, Zeldovich KB, Kowalik TF, Finberg RW, Wang JP, Jensen JD.** 2016. An experimental evaluation of drug-induced mutational meltdown as an antiviral treatment strategy. Evolution **70:**2470-2484.

45. **Ormond L, Liu P, Matuszewski S, Renzette N, Bank C, Zeldovich K, Bolon DN, Kowalik TF, Finberg RW, Jensen JD, Wang JP.** 2017. The Combined Effect of Oseltamivir and Favipiravir on Influenza A Virus Evolution. Genome Biol Evol **9:**1913-1924.

46. **Mair CM, Ludwig K, Herrmann A, Sieben C.** 2014. Receptor binding and pH stability - how influenza A virus hemagglutinin affects host-specific virus infection. Biochim Biophys Acta **1838:**1153-1168.

47. **Sandbulte MR, Westgeest KB, Gao J, Xu X, Klimov AI, Russell CA, Burke DF, Smith DJ, Fouchier RA, Eichelberger MC.** 2011. Discordant antigenic drift of neuraminidase and hemagglutinin in H1N1 and H3N2 influenza viruses. Proc Natl Acad Sci U S A **108:**20748-20753.

48. **Thoennes S, Li ZN, Lee BJ, Langley WA, Skehel JJ, Russell RJ, Steinhauer DA.** 2008. Analysis of residues near the fusion peptide in the influenza hemagglutinin structure for roles in triggering membrane fusion. Virology **370:**403-414.

49. **Reed ML, Yen HL, DuBois RM, Bridges OA, Salomon R, Webster RG, Russell CJ.** 2009. Amino acid residues in the fusion peptide pocket regulate the pH of activation of the H5N1 influenza virus hemagglutinin protein. J Virol **83:**3568-3580.

564 50. **Steinhauer DA, Wharton SA, Skehel JJ, Wiley DC.** 1995. Studies of the membrane fusion
565 activities of fusion peptide mutants of influenza virus hemagglutinin. J Virol **69:**6643-6651.
566 51. **Gething MJ, Doms RW, York D, White J.** 1986. Studies on the mechanism of membrane fusion:
567 site-specific mutagenesis of the hemagglutinin of influenza virus. J Cell Biol **102:**11-23.
568 52. **DuBois RM, Zaraket H, Reddivari M, Heath RJ, White SW, Russell CJ.** 2011. Acid stability of
569 the hemagglutinin protein regulates H5N1 influenza virus pathogenicity. PLoS Pathog **7:**e1002398.
570 53. **Matrosovich M, Tuzikov A, Bovin N, Gambaryan A, Klimov A, Castrucci MR, Donatelli I,**
571 **Kawaoka Y.** 2000. Early alterations of the receptor-binding properties of H1, H2, and H3 avian
572 influenza virus hemagglutinins after their introduction into mammals. J Virol **74:**8502-8512.
573 54. **Maines TR, Chen LM, Van Hoeven N, Tumpey TM, Blixt O, Belser JA, Gustin KM, Pearce**
574 **MB, Pappas C, Stevens J, Cox NJ, Paulson JC, Raman R, Sasisekharan R, Katz JM, Donis**
575 **RO.** 2011. Effect of receptor binding domain mutations on receptor binding and transmissibility of
576 avian influenza H5N1 viruses. Virology **413:**139-147.
577 55. **Chen LM, Blixt O, Stevens J, Lipatov AS, Davis CT, Collins BE, Cox NJ, Paulson JC, Donis**
578 **RO.** 2012. In vitro evolution of H5N1 avian influenza virus toward human-type receptor specificity.
579 Virology **422:**105-113.
580 56. **Stevens J, Blixt O, Tumpey TM, Taubenberger JK, Paulson JC, Wilson IA.** 2006. Structure and
581 receptor specificity of the hemagglutinin from an H5N1 influenza virus. Science **312:**404-410.
582 57. **Hensley SE, Das SR, Bailey AL, Schmidt LM, Hickman HD, Jayaraman A, Viswanathan K,**
583 **Raman R, Sasisekharan R, Bennink JR, Yewdell JW.** 2009. Hemagglutinin receptor binding
584 avidity drives influenza A virus antigenic drift. Science **326:**734-736.
585 58. **Yewdell JW, Caton AJ, Gerhard W.** 1986. Selection of influenza A virus adsorptive mutants by
586 growth in the presence of a mixture of monoclonal antihemagglutinin antibodies. J Virol **57:**623-
587 628.

588 59. **Hensley SE, Das SR, Gibbs JS, Bailey AL, Schmidt LM, Bennink JR, Yewdell JW.** 2011.
589 Influenza A virus hemagglutinin antibody escape promotes neuraminidase antigenic variation and
590 drug resistance. PLoS One **6:**e15190.
591 60. **Ginting TE, Shinya K, Kyan Y, Makino A, Matsumoto N, Kaneda S, Kawaoka Y.** 2012.
592 Amino acid changes in hemagglutinin contribute to the replication of oseltamivir-resistant H1N1
593 influenza viruses. J Virol **86:**121-127.
594 61. **Hooper KA, Bloom JD.** 2013. A mutant influenza virus that uses an N1 neuraminidase as the
595 receptor-binding protein. J Virol **87:**12531-12540.
596 62. **Neverov AD, Kryazhimskiy S, Plotkin JB, Bazykin GA.** 2015. Coordinated Evolution of
597 Influenza A Surface Proteins. PLoS Genet **11:**e1005404.
598 63. **Hendricks GL, Weirich KL, Viswanathan K, Li J, Shriver ZH, Ashour J, Ploegh HL, Kurt-**
599 **Jones EA, Fygenson DK, Finberg RW, Comolli JC, Wang JP.** 2013. Sialylneolacto-N-tetraose c
600 (LSTc)-bearing Liposomal Decoys Capture Influenza A Virus. J Biol Chem **288:**8061-8073.
601 64. **Schrodinger, LLC.** 2010. The PyMOL Molecular Graphics System, Version 1.3r1.
602 65. **Bowers KJ, Chow, E., Xu, H., Dror, R.O., Eastwood, M.P., Gregersen, B.A., Klepeis, J.L.,**
603 **Kolossvary, I., Moraes, M.A., Sacerdoti, F.D., Salmon, J.K., Shan, Y. and Shaw, D.E.** Scalable
604 Algorithms for Molecular Dynamics Simulations on Commodity Clusters, p 84. *In* (ed),
605 Proceedings of the 2006 ACM/IEEE conference on Supercomputing.
606 66. **Harder E, Damm W, Maple J, Wu C, Reboul M, Xiang JY, Wang L, Lupyan D, Dahlgren**
607 **MK, Knight JL, Kaus JW, Cerutti DS, Krilov G, Jorgensen WL, Abel R, Friesner RA.** 2016.
608 OPLS3: A Force Field Providing Broad Coverage of Drug-like Small Molecules and Proteins. J
609 Chem Theory Comput **12:**281-296.
610 67. **Leidner F, Kurt Yilmaz N, Paulsen J, Muller YA, Schiffer CA.** 2018. Hydration Structure and
611 Dynamics of Inhibitor-Bound HIV-1 Protease. J Chem Theory Comput **14:**2784-2796.

612 **Figure legends**

613 **Figure 1. Experimental design and viral amplification for passaging with the broadly neutralizing**
614 **antibody F10.** (A) Schematic of Experiment 1 and Experiment 2 trajectories. Cyan boxes indicate virus
615 that was passaged in the absence of antibody, with the top three passages as P1, P2, and P3, and additional
616 passages as labeled. Red and orange boxes indicate virus that was passaged in the presence of F10 broadly
617 neutralizing antibody (Experiments 1 and 2, respectively). Grey boxes indicate virus that was passaged in
618 the presence of 80R control antibody (Experiment 2). (B) Ratios of viral titers (output/input) plotted against
619 passage number. Experiment 1, upper panel. Experiment 2, lower panel.

620 **Figure 2. Mutations inferred to be evolving under positive selection in the presence of the broadly**
621 **neutralizing antibody F10.** (A) Trajectories of select mutations elicited by viral passaging with F10, with
622 80R control antibody, or without antibody, in terms of allele frequency. Mutations individually marked as
623 A638G and A639T (grey box) are in perfect linkage and yield N203V, as the wild-type sequence is GGT
624 **AAC** CAA (AAC = positions 638/639/640), protein: G**N**Q. The mutant sequence is GGT **GTC** CAA (GTC
625 = positions 638/639/640), protein: G**V**Q. (B) The posterior probability distribution of selection coefficients
626 (*s*) for the mutations for Experiments 1 & 2. Specific mutations are listed by influenza viral protein,
627 nucleotide change, and amino acid change. Seg = segment, Syn = synonymous. (C) Posterior distributions
628 of effective population size inferred from WFABC. The effective population size was estimated from time-
629 sampled genomic data assuming neutrality. For F10-treated (F10) and control (ctrl), we respectively
630 estimated N_e to be 208 (99% highest posterior density (HPD) interval: [162, 249]) and 440 (99% HPD
631 interval: [350, 512]).

632 **Figure 3. Growth of WT and individual mutant viruses in the presence of F10 or oseltamivir.** (A)
633 Viral titers for WT and mutant viruses (HA, NA, and HA-NA double mutant) were grown in the indicated
634 concentrations of F10 and quantified by plaque assay. (B) Viral response to the NA inhibitor oseltamivir

was measured for the resistance mutation H275Y^{NA} compared to wild type and the mutation E329K^{NA}. Error bars indicate the standard deviation.

Figure 4. Viral fitness was estimated by plaque size. Plaque diameters of HA and NA mutant viruses in the absence of F10 (n=20 per virus). Error bars indicate the standard deviation. A one-way ANOVA multiple comparisons test was performed (***, $P < 0.001$; ****, $P < 0.0001$).

Figure 5. Escape mutations identified in the F10 trajectories mapped onto the structure of HA. The HA trimer is displayed in gray surface representation (PDB ID: 3FKU). The F10 epitope (or footprint) on the HA stem is displayed as sticks and colored according to degree of contacts with the antibody F10, with residues with the greatest contacts in green, intermediate in cyan, and smallest contacts in navy blue. The fusion peptide is in orange stick representation between the F10 epitope (footprint), and the locations of escape mutations are labeled.

Figure 6. The N460S^{HA} mutation is located adjacent to the fusion peptide. (A) The structure of HA monomer at neutral pH is shown with respect to the viral envelope and endosomal membrane (PDB ID: 3FKU). The HA1 subunit, which forms the head of HA, is shown in blue, the HA2 subunit, which forms the stem of HA, is in grey, and the fusion peptide is colored red. (B) The location of mutation N460S is circled on the structure of HA at neutral pH with the F10 epitope colored as in Figure 5. (C) A zoom-in view of the stem region harboring N460S, and (D) the hydrogen bond between N460 and the fusion peptide indicated with a black dashed line. (E) At acidic pH, the fusion peptide dissociates from the stem of HA and inserts into the endosomal membrane (PDB ID: 1HTM). (F) The structure of HA2 at acidic pH is shown, where residue N460 is exposed to the surface and is colored yellow (PDB ID: 1HTM). (G) and (H) show this residue in more detail.

Figure 7. S123G^{HA} is located in a hinge region of conformational change in an early fusion intermediate of HA1. (A) The surface representation of HA structure at neutral pH where residue S123 is circled and surrounding residues 115-129 are displayed in green (PDB ID: 3QQB). (B) The structure of an

early fusion intermediate of HA at acidic pH where residue S123 is circled and residues 115-129 colored yellow (PDB ID: 3QQO). (C) A detailed view of S123 at neutral pH with surrounding residues colored in green to show the early conformational changes that occur in HA1 during fusion. S123 is located in a hinge region of conformational change in HA1, and the direction of the conformational changes that occur at acidic pH is indicated with red arrows (PDB ID: 3QQB). (D) The resulting structure of the early fusion intermediate of HA is shown in yellow (PDB ID: 3QQO).

Figure 8. The N203V^{HA} mutation is located in the receptor binding site. (A) The head region of HA is represented by a grey surface and the location of mutation N203V is labeled with a circle and colored yellow. The human receptor analog LSTc is shown as gold sticks (PDB ID: 2WRG). (B) N203V is located in the HA receptor binding site and forms a hydrogen bond with the human receptor analog LSTc. The hydrogen bond is shown with a black dashed line connecting the side chain oxygen atom of N203 with a nitrogen atom on LSTc.

Figure 9. The dynamics and electrostatic surface of WT and E329K^{NA}. The root-mean-squared-fluctuations (RMSF) of (A) WT and (B) E329K NA during 100 ns MD simulations. The residues are colored on a rainbow scale from blue to red for increasing RMSF values; hence, warmer colors indicate residues with more backbone fluctuations. The radius of the cartoon representation also indicates the RMSF values: the thicker the tube, the higher the RMSF values. The oseltamivir from pdb:3cl2 (black sticks) is displayed solely to indicate the active site on all four NA molecules. (C,D) The electrostatics surface for the final frame from MD simulations of (C) WT and (D) E329K^{NA}. The residues are colored on a rainbow scale from blue (positive) to red (negative).

680 **Tables**

681 **Table 1. Sites inferred to be evolving under positive selection (99% posterior probability of $s > 0$)**

Experiment 1	**Segment**	**Protein**	**Nucleotide change**	**Amino acid change**
	3	PA	T106C	L28P
	4	HA	A398G	S123G
	4	HA	G1147A	synonymous
	4	HA	A1410G	N460S
	5	NP	T1148C	synonymous
	6	NA	G1004A	E329K
Experiment 2	**Segment**	**Protein**	**Nucleotide change**	**Amino acid change**
	2	PB1	G1950A	A643T
	4	HA	A638G	N203V
	4	HA	A639T	
	6	NA	G1004A	E329K

682

683

684

685 **Table 2. F10 effective concentration (EC) values for influenza A/Brisbane/59/2007**

Variant	**Epitope region**	**Likely function**	**F10 EC_{50} (±S.D.)**	**F10 EC_{90} (±S.D.)**
WT	--	--	0.37 ± 0.04	0.49 ± 0.04
$S123G^{HA}$	Head	Modulate fusion pH	0.92 ± 0.12	1.21 ± 0.10
$N460S^{HA}$	Stem	Modulate fusion pH	0.77 ± 0.08	0.91 ± 0.26
$N203V^{HA}$	Head	Receptor binding specificity	0.68 ± 0.03	0.82 ± 0.08
$E329K^{NA}$	Distal to active site	Antigenic drift/modulate active site	0.29 ± 0.01	1.21 ± 0.10
$H275Y^{NA}$	Near active site	Resistance to oseltamivir	0.41 ± 0.01	0.52 ± 0.01
$E329K^{NA}$_ $N203V^{HA}$	See above	See above	0.70 ± 0.06	1.18 ± 0.13

686 Note: Data shown in this table are from one experiment. A second independent experiment to determine EC

687 values yielded similar results.

Figure 1

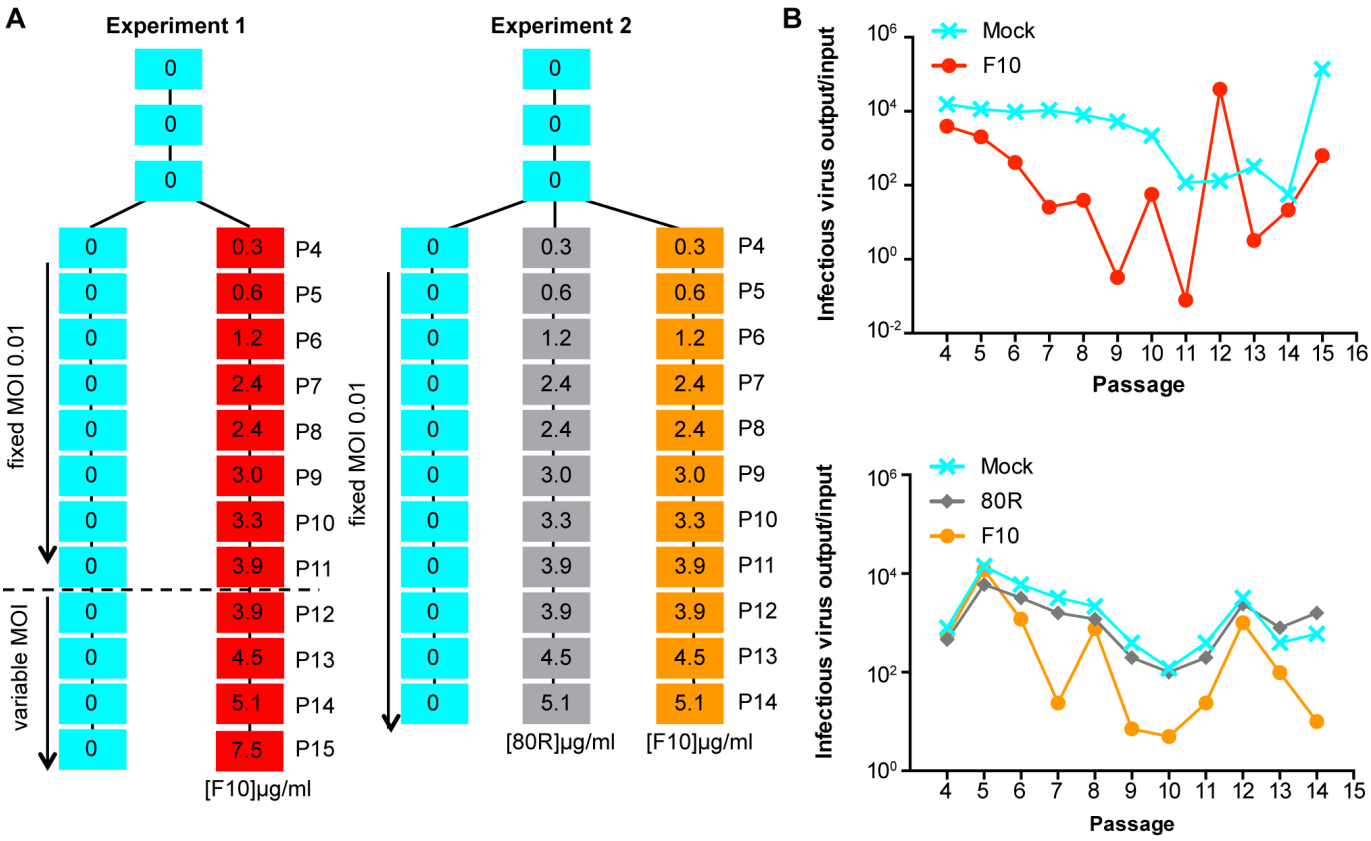

Figure 2

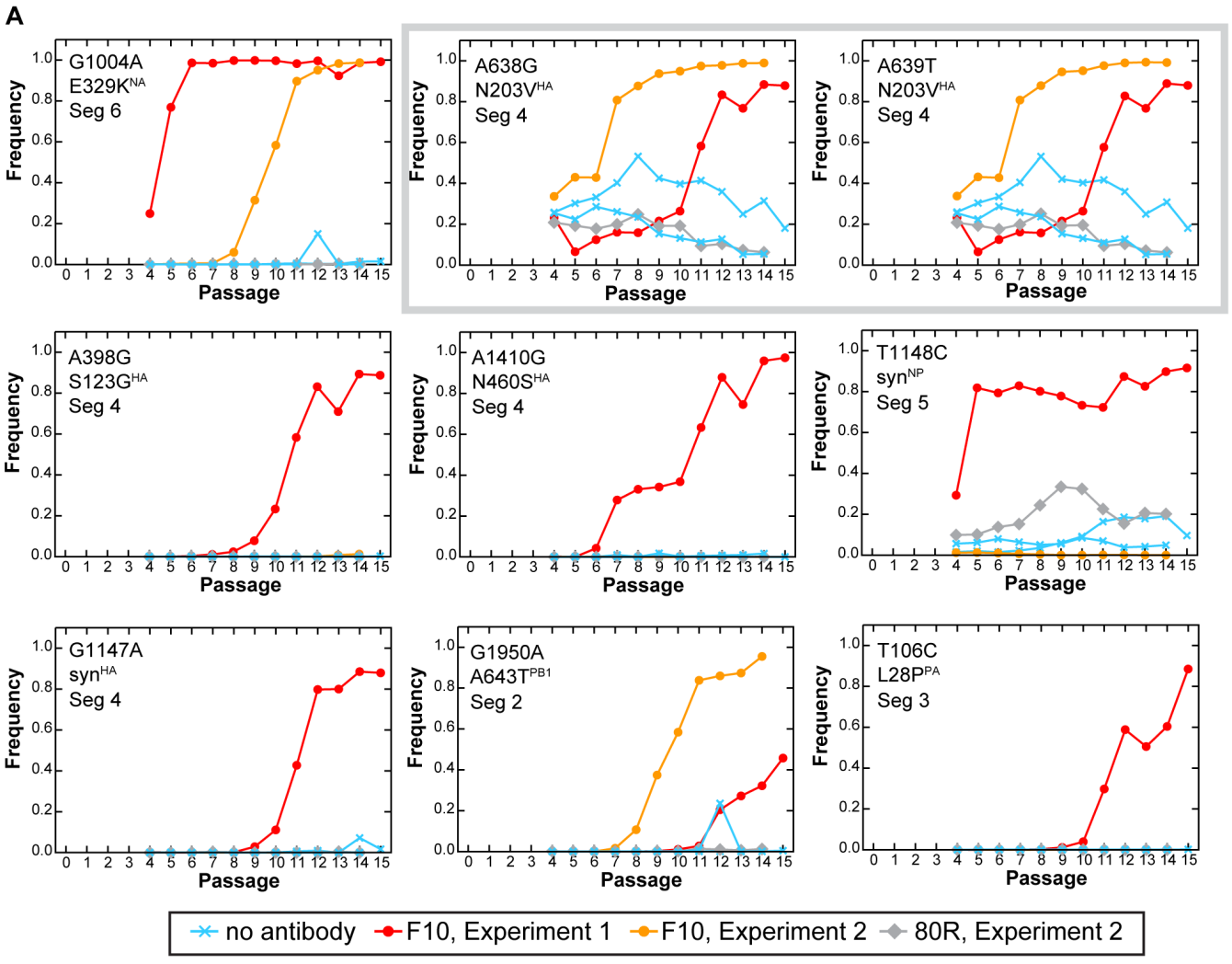

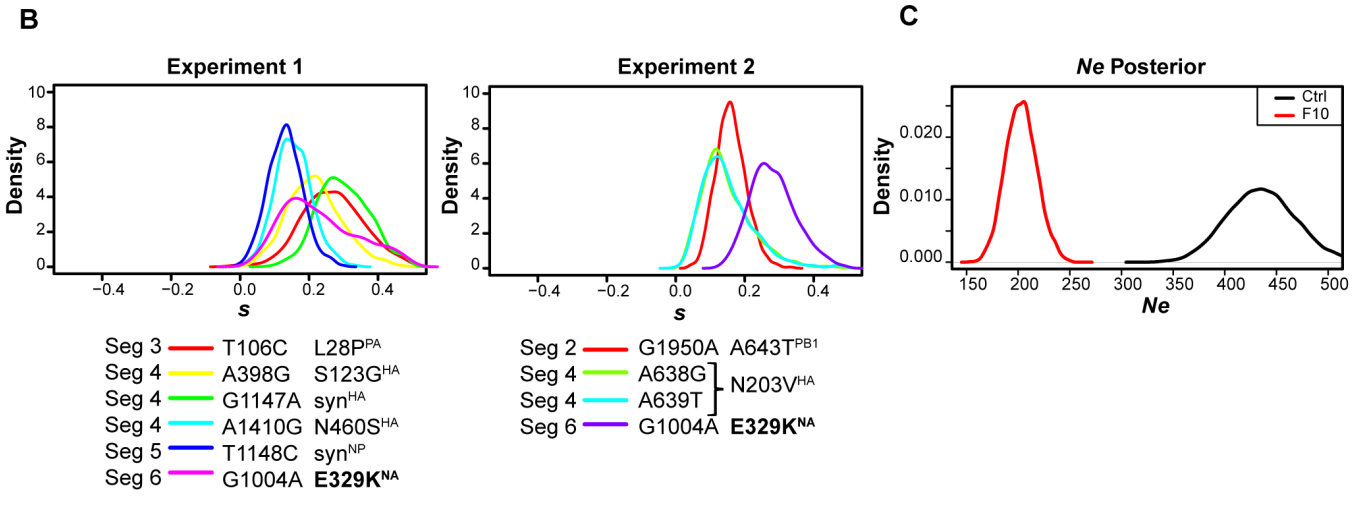

Figure 3

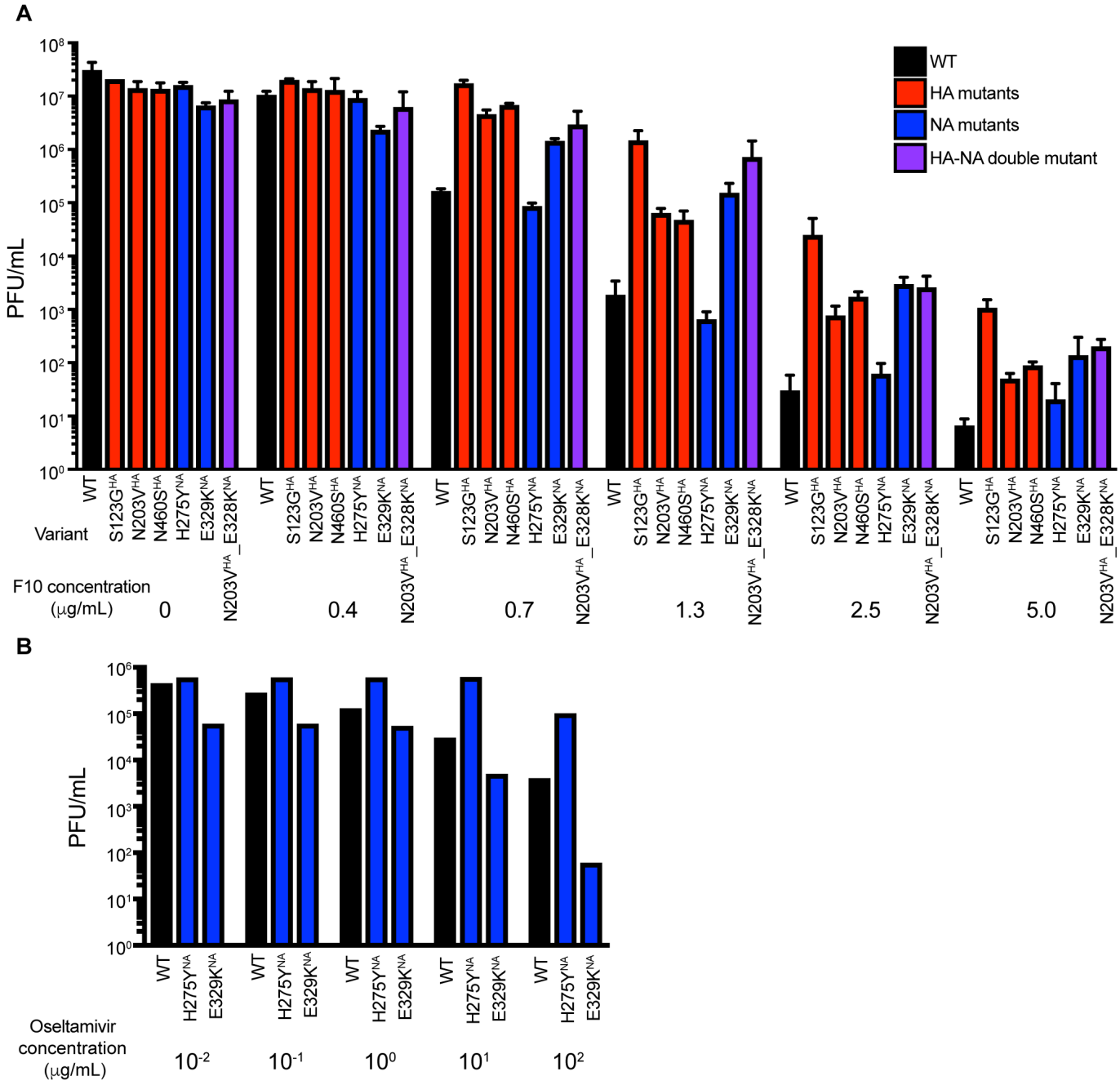

Figure 4

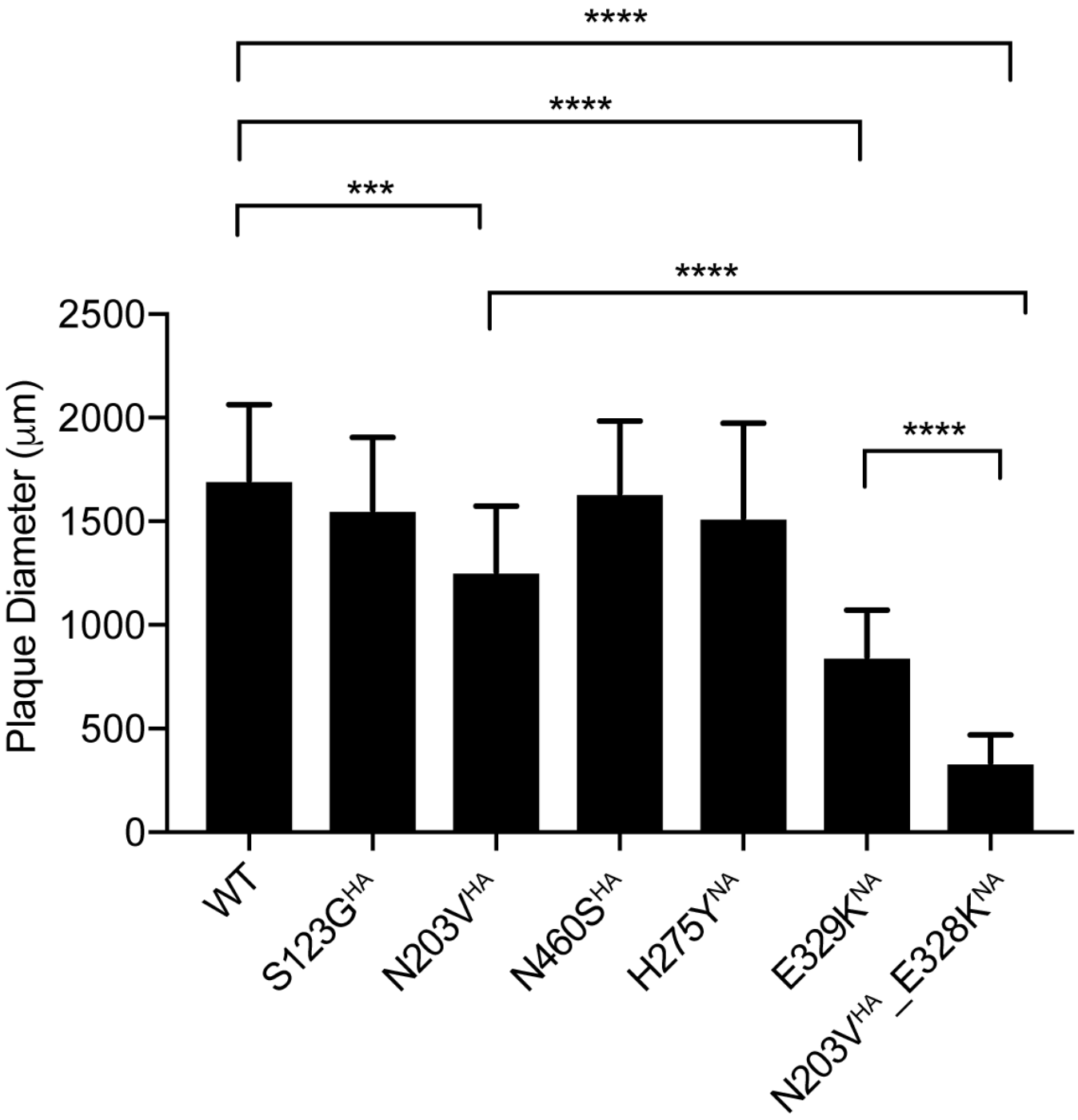

Figure 5

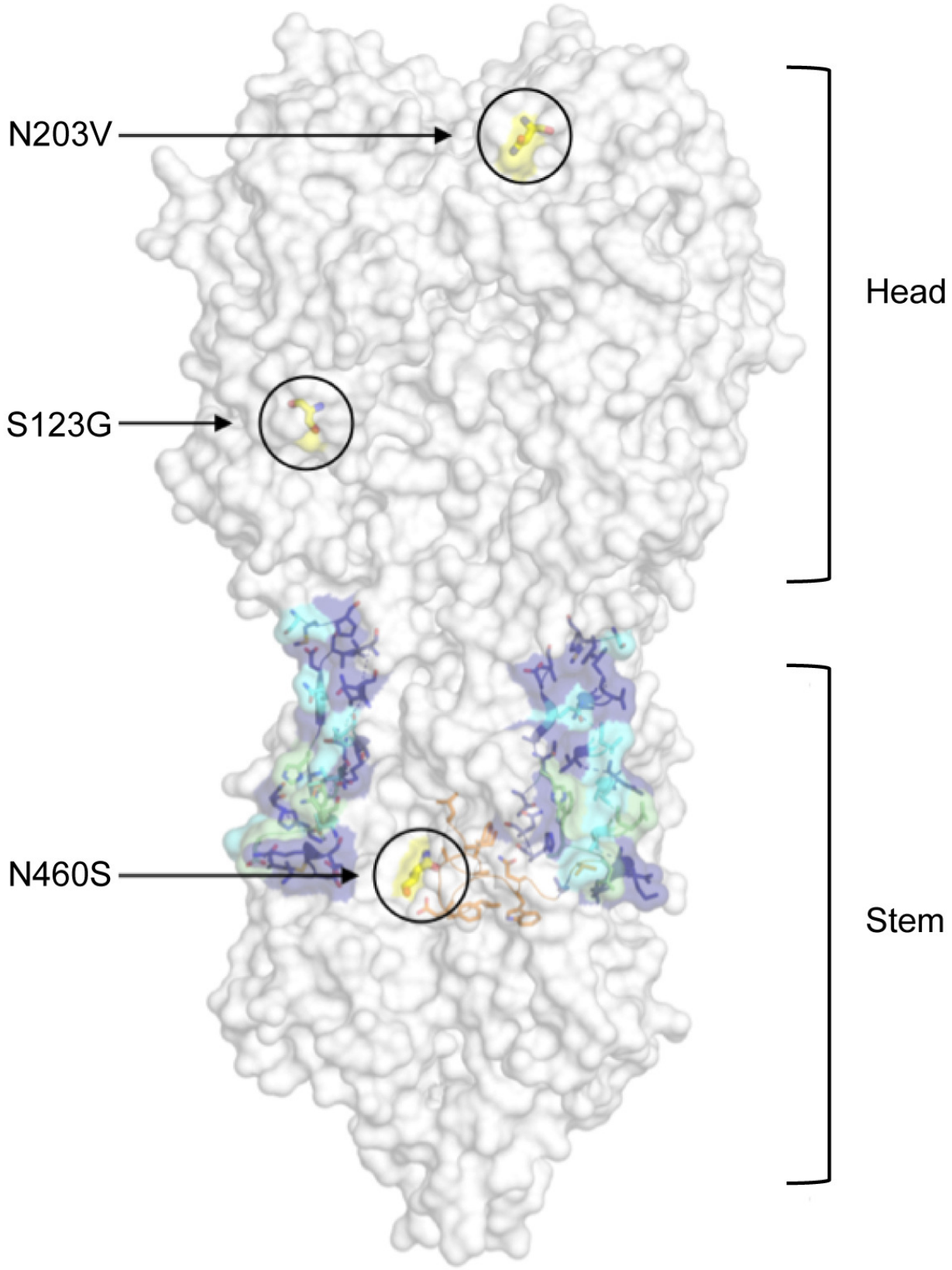

Figure 6

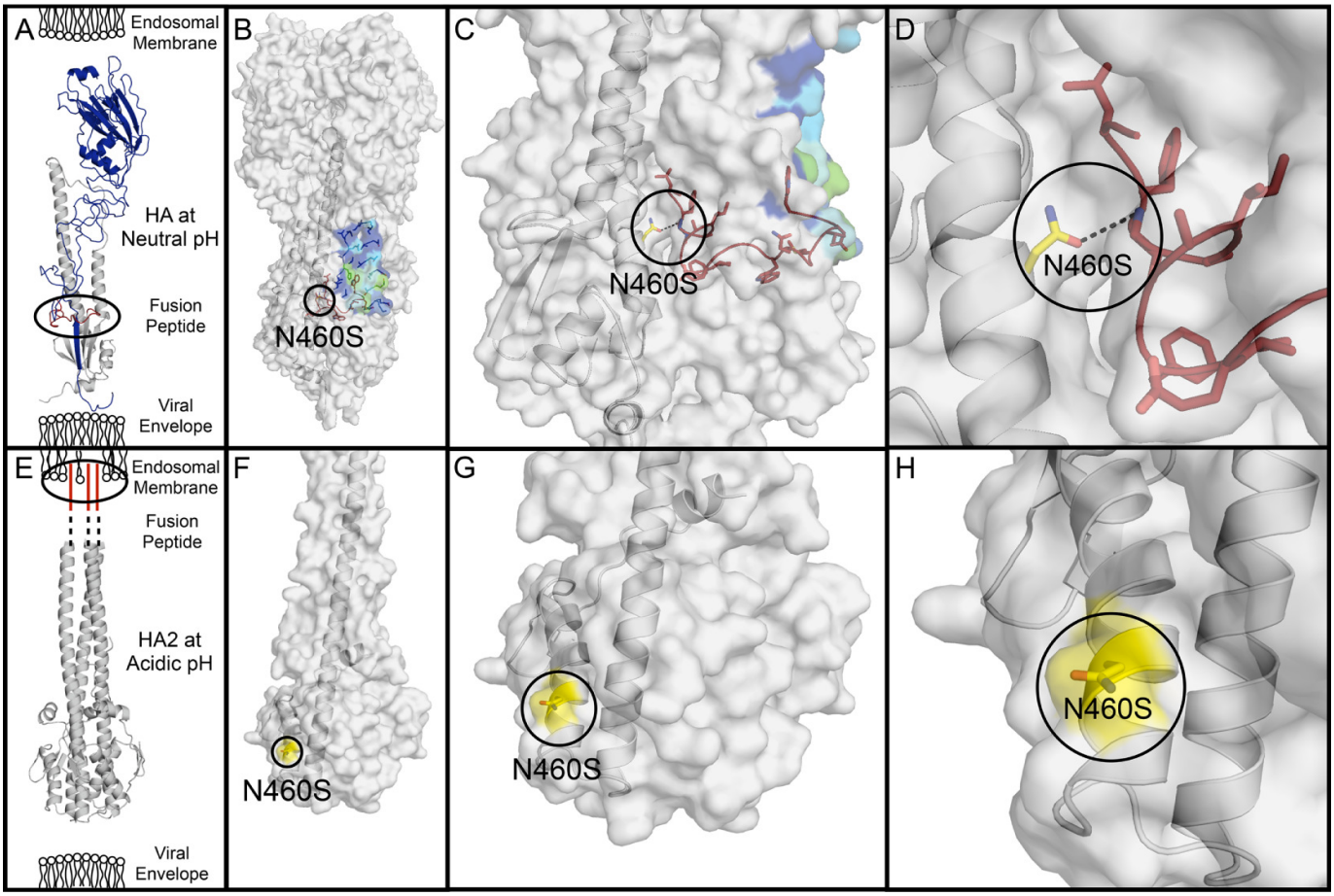

Figure 7

Figure 8

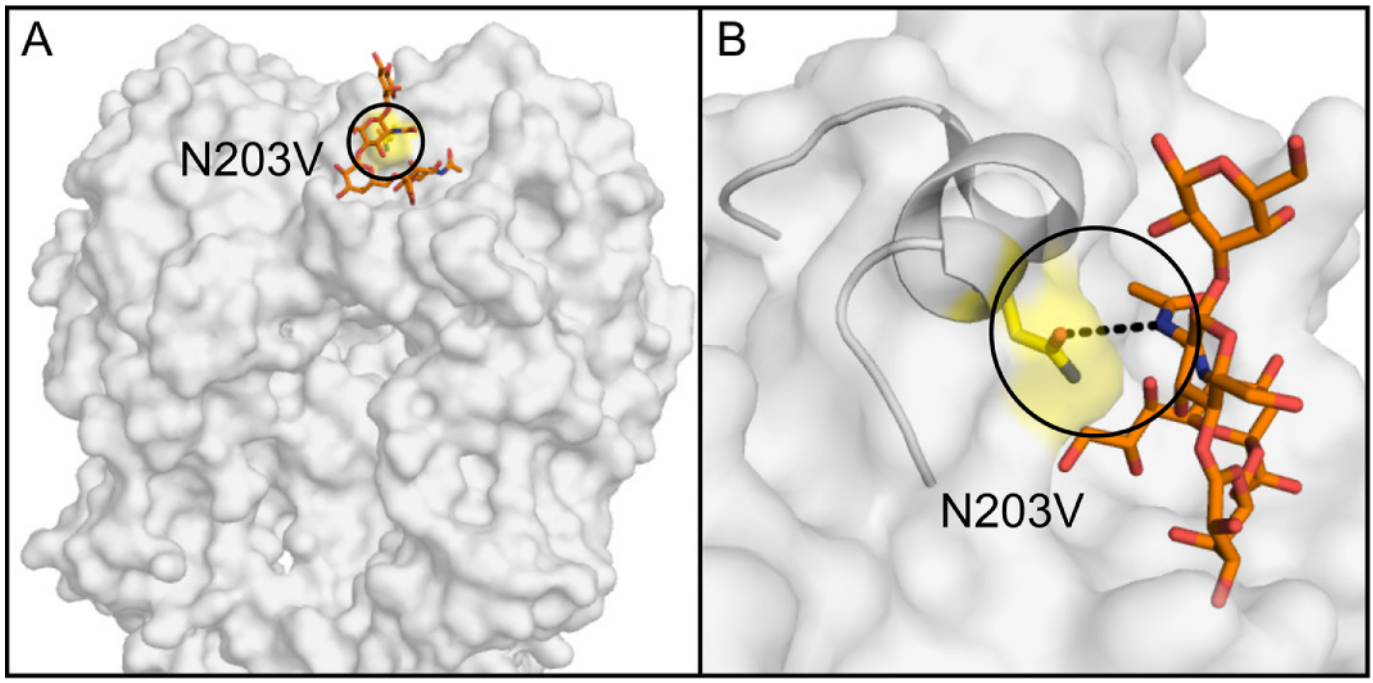

Figure 9